THE JOURNAL OF PHYSICAL CHEMISTRY C

Article

pubs.acs.org/JPCC

Metal Doping of $BiVO_4$ by Composite Electrodeposition with Improved Photoelectrochemical Water Oxidation

Sung Ki Cho, Hyun S. Park, Heung Chan Lee, Ki Min Nam, and Allen J. Bard*

Center for Electrochemistry, Department of Chemistry and Biochemistry, The University of Texas at Austin, Austin, Texas 78712, United States

Supporting Information

ABSTRACT: We report that oxide composite electrodeposition can be used for the facile preparation of metal-doped $BiVO_4$ photoelectrodes for photoelectrochemical water oxidation. The photoactivity of electrodeposition film was improved by the addition of a small amount of tungstic acid particles during the electrodeposition. These particles are incorporated in the deposit and finally generate tungsten-doped bismuth vanadate. The suspended particles in the plating solution were electrostatically attracted to the cathode and accordingly incorporated into the deposit (electrostatic deposition). WO_3 nanoparticles (NPs) can be used instead of tungstic acid, to yield a $BiVO_4$ with different properties. Enhanced photoelectrochemical (PEC) water oxidation was confirmed via scanning electrochemical microscopy (SECM) by detecting increased oxygen evolution with using optical fiber incorporating a ring electrode.

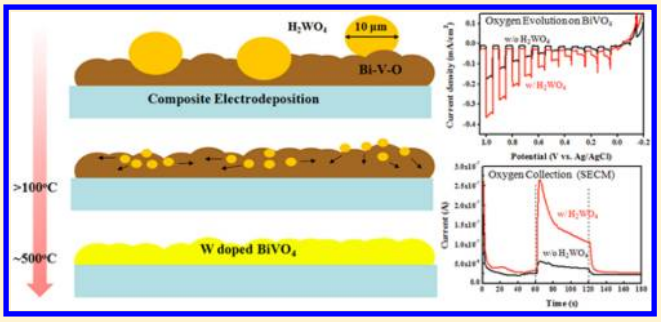

INTRODUCTION

$BiVO_4$ was reported to be an n-type photocatalyst by Kudo et al. in 1999,[1] and many studies have been reported using this material for water oxidation and the PEC decomposition of organic materials.[2,3] Photocatalysts for water oxidation have been extensively studied as a component in systems for water splitting to produce hydrogen as a solar fuel.[4−6] Among the many candidates for water oxidation photocatalysts, metal oxides have been extensively investigated because of their good physical and chemical stability. For example, extensive studies of TiO_2 and attempts to modify its large band gap have been reported since Fujishima and Honda suggested the possible photolysis of water using TiO_2 electrodes.[7−10] Other metal oxides, e.g., WO_3,[11−13] Fe_2O_3,[14−16] or $BiVO_4$ as mentioned above, have also been widely studied. However, no simple oxide has yet been discovered with sufficient efficiency and stability as a photocatalyst to achieve practical water splitting.[17]

Monoclinic $BiVO_4$, which has been considered as the highly active photocatalyst among its many polymorphs,[18] has a band gap size of 2.4−2.5 eV, so it can absorb the visible portion of the solar energy so as to have a theoretical efficiency of 9% for solar-to-chemical conversion.[19] However, the short carrier diffusion lengths and significant recombination of photon-generated electron−hole pairs limit the photoactivity of $BiVO_4$.[20] To enhance the activity of $BiVO_4$ for water oxidation, there have been many studies to reduce electron−hole recombination: (a) metal dopants added into $BiVO_4$ to increase the donor density and increase carrier mobility, e.g., W-, Mo-, or P-doped $BiVO_4$;[21−23] (b) semiconductor layers added, e.g., at the FTO/$BiVO_4$ interface, decrease surface recombination of an electron with a surface trapped-hole, e.g., with WO_3 and SnO_2 as the barrier layers;[24−27] (c) treatments of $BiVO_4$ at the liquid surface, e.g., the addition of electrocatalysts, to increase the rate of water oxidation reactions.[28−30] Further, the relationship between photocatalytic activity and many different preparation methods of the metal oxide has been reported.[31,32]

Among various preparation methods such as chemical bath deposition,[33] precipitation,[34] hydrothermal,[35] spray pyrolysis,[36] metal−organic decomposition,[20] and electrochemical approaches (e.g., electrodeposition),[29,37] electrodeposition has the advantage of being a simple, low cost process, that is compatible with various size surfaces, but the precise control of adding effective dopant elements to the film is challenging. In the case of electrochemically grown hematite, which is formed by the reduction of H_2O_2 in the presence of Fe^{3+}, its doping with metals such as Pt, Mo, and Cr was accomplished by the reduction of the metal ion with consequent codeposition of metal in the film; these improve the photoactivity of hematite.[16,38] However, the doping of semiconductors via metal codeposition cannot be simply applied to the preparation of semiconductors such as $BiVO_4$, TiO_2, and WO_3, which are generally synthesized by an electrochemical oxidation reaction where the metal would not codeposit simultaneously unless the oxidized metal ion formed a precipitate on the deposit surface.

Received: August 28, 2013
Revised: October 7, 2013
Published: October 11, 2013

During electrodeposition, the deposited film basically consists of elements reduced or oxidized from reactants in the electrolyte. Moreover, ions in the electrolyte can be captured in the deposited film at the few ppm level.[39] In some cases, electrochemically inert solid particles suspended in the electrolyte can be incorporated into the electrodeposited metal or oxide film to result in the formation of a matrix composite film, which can also have improved physical properties (e.g., wear and corrosion resistance),[40,41] as well as improved electrocatalytic properties, e.g., for the oxygen or hydrogen evolution reaction.[42]

Incorporation of particles into the deposited film has been explained by their electrostatic (electrophoretic) attraction and adsorption.[41,43,44] Particles are transported to the electrode surface by forced convection, migration, and diffusion and are subsequently adsorbed on the surface.[41,43,44] There are thus many important factors, such as particle amount, agitation, and pH of the deposition medium, that are important in composite deposition.

Herein, we employ the composite deposition as a facile method to prepare a doped bismuth vanadate ($BiVO_4$) for the improved photoelectrochemical water oxidation. Recently, Seabold et al.[29] reported an electrochemical route for the formation of $BiVO_4$ film by oxidation of VO^{2+} in the presence of Bi^{3+} in the plating solution followed by heat treatment. We show here that adding tungstic acid (H_2WO_4 or $WO_3{\cdot}H_2O$) or tungsten oxide to the plating solution results in the formation of W-doped $BiVO_4$. The photogeneration of oxygen was examined by scanning electrochemical microcopy (SECM) modified by replacing the ultramicroelectrode (UME) tip with an optical fiber. SECM can show the improved photoactivity by comparing photocurrent and the collection of photogenerated oxygen produced at the photocatalyst substrates.[45,46]

EXPERIMENTAL SECTION

Materials. $Bi(NO_3)_3{\cdot}5H_2O$ (>98%, MCB Manufacture Chemists. Inc.), $VOSO_4{\cdot}H_2O$ (17−23% V, Acros Chemicals), CH_3COONa (99.3%, Fisher Scientific), H_2WO_4 (99%, Strem Chemicals), WO_3 (99%, diameter ≤ 20 μm, Sigma-Aldrich), WO_3 nanoparticle (diameter < 100 nm, primary particle diameter 20 nm, Sigma-Aldrich), $Na_2WO_4{\cdot}2H_2O$ (99%, Sigma-Aldrich), NaH_2PO_4 (99.5%, Fisher Scientific), Na_2HPO_4 (99.9%, Fisher Scientific), Na_2SO_3 (99.4%, Fisher Scientific), and Na_2SO_4 (99.3%, Fisher Scientific) were used as received. Milli-Q deionized (DI) water was used to prepare aqueous solutions for electrochemistry experiments. F-doped tin oxide (FTO) coated glass (<14 Ω, 15 mm × 20 mm, Pilkington, Toledo, OH) was used as a substrate.

Preparation of BiVW-O Film. All of the $BiVO_4$ films were prepared by the previously reported electrodeposition method.[29] The plating electrolyte was 10 mM $Bi(NO_3)_3{\cdot}5H_2O$, 35 mM $VOSO_4{\cdot}5H_2O$, 2 M CH_3COONa, and various amounts of H_2WO_4, and its pH was adjusted to 5 by adding concentrated HNO_3 dropwise. Electrodeposition was performed on the FTO substrate (1 cm^2) at room temperature by applying 1.9 V (vs Ag/AgCl reference electrode) for 1000 s, and Pt wire (1 mm dia.) was used as a counter electrode. A gray amorphous film that consisted of Bi−V−O was formed after electrodeposition and, following annealing (550 °C for 3 h, 1 °C/min increment from room temperature), produced a yellow crystalline $BiVO_4$ layer.

PEC Measurements of $BiVO_4$ Films. The photoactivity of the deposited $BiVO_4$ was measured in a photoelectrochemical cell. The prepared films were used as working electrodes (0.27 cm^2) exposed to electrolyte solution and irradiation. All measurements were carried out in a borosilicate glass cell with a Pt counter electrode and Ag/AgCl reference electrode. UV−vis light was irradiated through the electrolyte solution using full output of the Xe lamp with an incident light intensity of about 100 mW/cm^2. A 420 nm cutoff filter (WBF-3, Oriel, Darmstadt, Germany) was used for only visible irradiation. The electrolyte was 0.1 M Na_2SO_3/0.1 M Na_2SO_4 solution or 0.2 M sodium phosphate buffer (pH 7).

Characterization. Glancing incidence angle X-ray diffraction (XRD) measurements were performed by using D8 ADVANCE (Bruker, Fitchburg, WI) equipped with a Cu Kα radiation source where the incident angle was 0.4°. X-ray photoelectron spectroscopy (Kratos XPS, Kratos Analytical Ltd., UK) equipped with a monochromatic Al X-ray source was also performed. $BiVO_4$ films were also characterized by scanning electron microscopy (SEM, Quanta 650 FEG, FEI Company, Inc., Hillsboro, OR) and by energy dispersive spectroscopy (EDS) (XFlash Detector 5010, Bruker, Fitchburg, WI).

Pt-Ring Optical Fiber Electrode. A Pt-ring modified optical fiber was fabricated using a commercial Au-coated optical fiber (Fiberguide Industries, Inc., Stirling, NJ) as described earlier.[45] The Au-coated optical fiber was sealed in a borosilicate glass tube as used in the preparation of UMEs for SECM experiments.[47] The sizes of the Au-ring optical fiber used were as follows: inner diameter (dia.) of the optical fiber, 200 μm; inner diameter of the Au ring, 240 μm; outer diameter of the Au ring, 275 μm; diameter of the whole optical fiber including the glass insulator, 600 μm. Pt was electrodeposited on the Au ring electrode from a 1.0 mM K_2PtCl_6/0.1 M Na_2SO_4 aqueous solution to promote the oxygen reduction reaction.

RESULTS AND DISCUSSION

$BiVO_4$ Deposited with Tungstic Acid. H_2WO_4 is the hydrated form of WO_3, insoluble in neutral aqueous solutions, and electrochemically inert, so it does not affect the plating step. However, the $BiVO_4$ film grown with a H_2WO_4 particle suspension showed a significantly improved photocurrent. Figure 1 shows the linear sweep voltammograms of $BiVO_4$ films electrodeposited with and without H_2WO_4 particles under UV−vis irradiation in 0.1 M Na_2SO_3/0.1 M Na_2SO_4 solution for sulfite oxidation (Figure 1a) and in 0.2 M sodium phosphate buffer (pH 7, Figure 1b) for water oxidation. The photocurrents for the oxidation of sulfite and water increased about 2.5 times with the addition of H_2WO_4 (25 mg/L). This improvement of photoactivities is similar to that of a W-doped $BiVO_4$ film prepared by drop casting reported previously[21,22] and the photocurrent of the electrodeposited film is almost the same as that previously reported under the same measurement conditions.

Film Characterization. The improvement with H_2WO_4 is strongly related to W-doping, i.e., incorporation of W in $BiVO_4$ lattice,[22] although composites of $BiVO_4$ also show improved PEC properties.[26] Thus, the electrodeposited films were examined by several techniques. In SEM analysis (Supporting Information Figure S1), a morphological difference between $BiVO_4$ films grown with and without H_2WO_4 was not observed, which means that the addition of H_2WO_4 did not affect the surface sites of the photocatalytic reaction. XPS analysis (Figure 2) showed W 4f spectra from $BiVO_4$ films electrodeposited

dx.doi.org/10.1021/jp408619u | J. Phys. Chem. C 2013, 117, 23048−23056

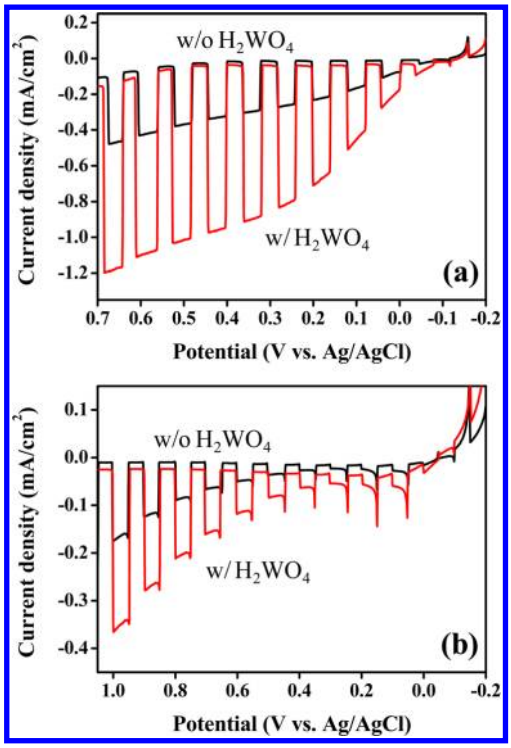

Figure 1. Linear sweep voltammograms of $BiVO_4$ electrodeposited with and without H_2WO_4 in (a) 0.1 M Na_2SO_3/0.1 M Na_2SO_4 aqueous solution and (b) 0.2 M sodium phosphate buffered aqueous solution (pH 7) with chopped light under UV−visible irradiation. Intensity of light from a full xenon lamp was about 100 mW/cm^2, and the scan rate was 20 mV/s.

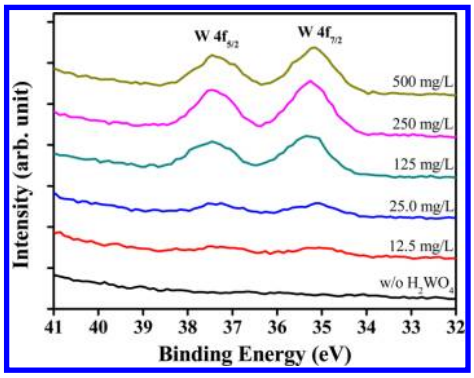

Figure 2. W 4f X-ray photoelectron spectrum of $BiVO_4$ films electrodeposited with various amount of H_2WO_4 in the plating solution.

with different amounts of H_2WO_4 particles in the plating solution. According to the XPS analysis, W is in the fully oxidized state (W^{6+}), and the peak intensity of W 4f increased with the amount of H_2WO_4 in the solution.

Incorporation of W in the film was also verified by XRD analysis (Figure 3). Clear diffraction patterns of the monoclinic scheelite-like $BiVO_4$ (PDF #14−0688) were obtained from the prepared films. The addition of H_2WO_4 in the solution up to 25 mg/L did not result in the formation of a separate W phase such as WO_x or Bi_2WO_6; rather a shift and merger of peaks at about 34° and 47° were observed. These peak shifts and the relevant crystal deformations are critical evidence of W-doping in $BiVO_4$ film.[21,22] W-doping is known to increase the carrier density of $BiVO_4$ as verified via Mott−Schottky plot

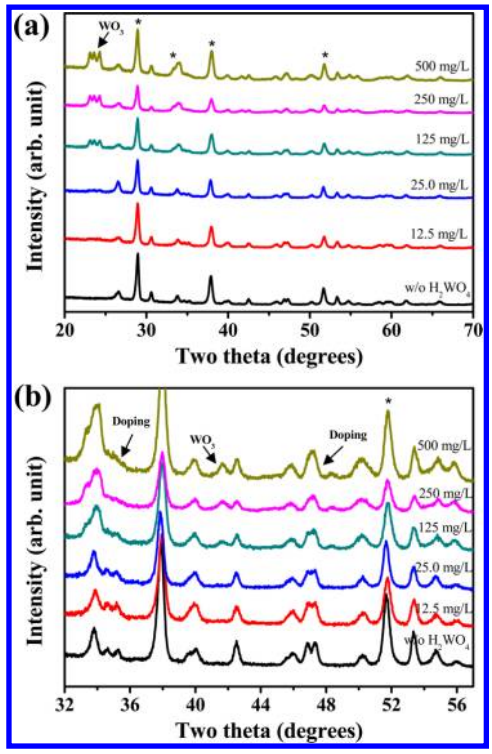

Figure 3. (a) X-ray diffraction spectrum of $BiVO_4$ films electrodeposited on FTO substrate (*) with various amounts of H_2WO_4 in the plating solution and (b) the same with small angle range.

analysis,[21,22] and the same results were observed on $BiVO_4$ film electrodeposited with H_2WO_4 (Supporting Information Figure S2). Further addition of H_2WO_4 produces a monoclinic WO_3 secondary phase, which appears at 23° and 41.5° in the diffraction pattern as well as crystal deformation in the $BiVO_4$ film, so these films were identified as composites of WO_3 and W-doped $BiVO_4$. Diffraction peaks from monoclinic WO_3 (crystal size: 18.4 ± 0.9 nm calculated by Scherrer equation) in the deposited film became more intense as the amount of H_2WO_4 increased in the precursor solution. W incorporation also affects the UV−vis absorption spectra of films (Figure 4). The difference in the absorption of light in visible range (>420 nm) was not significant with the addition of H_2WO_4, as observed previously.[22] The absorption at shorter wavelengths

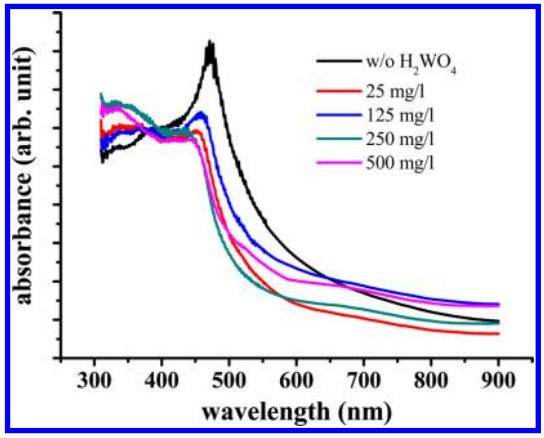

Figure 4. UV−visible absorption spectra obtained from $BiVO_4$ films electrodeposited with various amounts of H_2WO_4 in the plating solution. The thickness was around 200 nm for all electrode films.

dx.doi.org/10.1021/jp408619u | J. Phys. Chem. C 2013, 117, 23048−23056

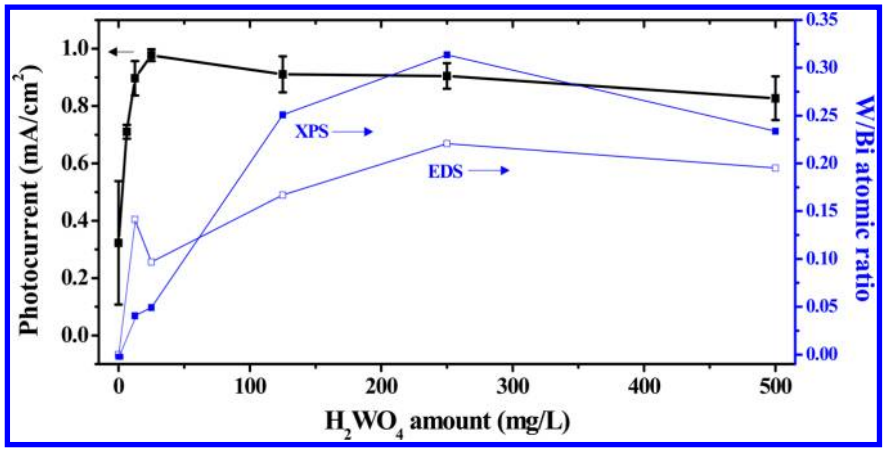

Figure 5. Relationship between the amount of H_2WO_4 particle in the plating solution and the photocurrent measured at 0.4 V (vs Ag/AgCl) in 0.1 M Na_2SO_3/0.1 M Na_2SO_4 aqueous solution with 100 mW/cm^2 UV−visible light irradiation (black line), and the relationship between the amount of H_2WO_4 and the atomic concentration ratio of tungsten to bismuth in the $BiVO_4$ film measured via EDS and XPS (blue line). The slight decrease in W/Bi ratio with increasing H_2WO_4 results from increased particle aggregation at larger amounts of tungstic acid.

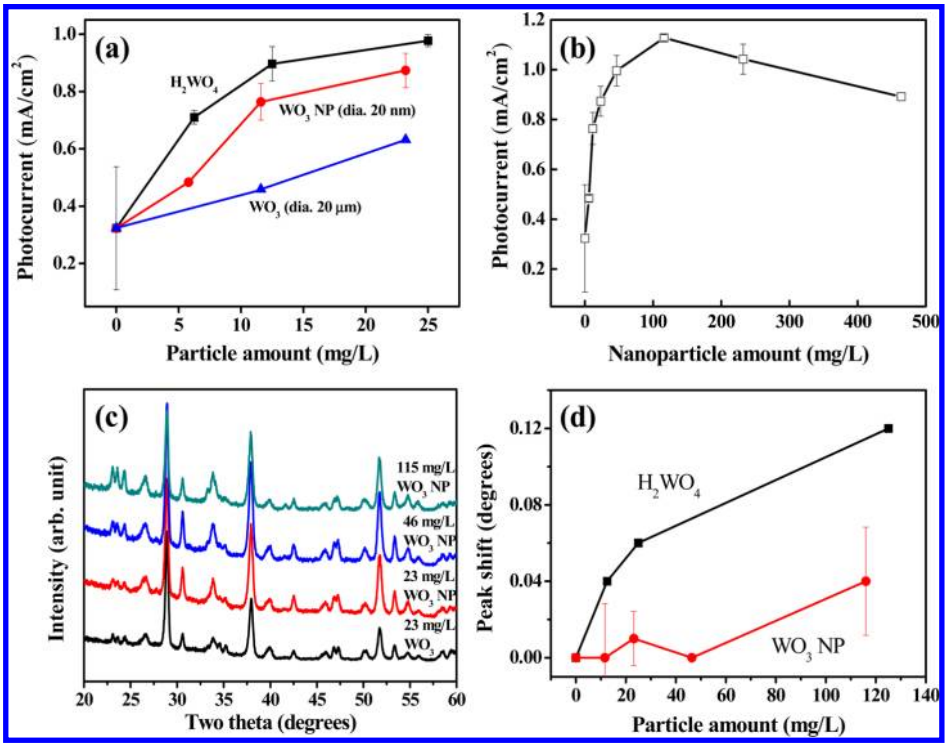

Figure 6. (a,b) Photocurrents (at 0.4 V vs Ag/AgCl in 0.1 M Na_2SO_3/0.1 M Na_2SO_4 aqueous solution, 100 mW/cm^2 UV−visible light) and (c) X-ray diffraction spectrum of $BiVO_4$ films electrodeposited with various amount of WO_3 bulk particles (diameter ≤ 20 μm) and WO_3 nanoparticles (primary particle diameter 20 nm). (d) The peak shift of characteristic diffraction peak of $BiVO_4$ (at 46.86°) with amount of H_2WO_4 or WO_3 particles added to electrodeposition solution.

increased due to the increase of WO_3 that absorbs in this region ($E_g \approx 2.7-2.8$ eV) in the composite.

Figure 5 shows the relationship between the amounts of H_2WO_4 used during the deposition and the atomic concentration of W in the film and the corresponding photocurrent. The atomic concentration was estimated from XPS and EDS analyses, and the photocurrents were measured in 0.1 M Na_2SO_3/0.1 M Na_2SO_4 at 0.4 V (vs Ag/AgCl) under UV−vis irradiation. The atomic concentrations from XPS analysis were slightly different from those from the EDS analysis, but their trends are the same, showing a gradual increase followed by saturation. The photocurrent increased sharply with the addition of H_2WO_4 and showed the highest value (0.98 mA/cm^2) at around 25 mg/L, which is the maximum amount that shows W doping without the formation of separate WO_3 phase in the film. The atomic ratio of W to Bi at the maximum photocurrent is 0.05 from XPS or 0.1 from EDS, which are similar to the previously reported value (0.11).[21,22] Beyond the maximum at 25 mg/L, the photocurrent decreased gradually, indicating WO_3 in W-doped $BiVO_4$ did not contribute to the further increase in the photoresponse. In fact, the visible light (>420 nm) photoresponse of the composite of WO_3 and W-$BiVO_4$ was similar to that of the W-doped $BiVO_4$ without the WO_3 phase

dx.doi.org/10.1021/jp408619u | J. Phys. Chem. C 2013, 117, 23048−23056

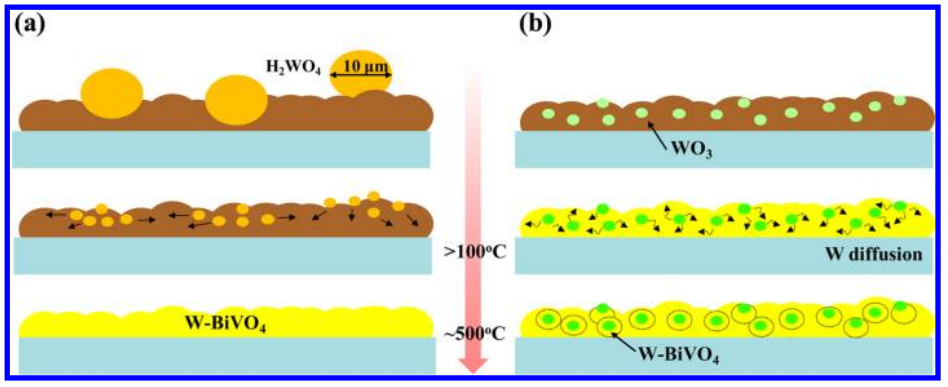

Figure 7. Illustration of the formation of W-$BiVO_4$ from films electrodeposited with (a) H_2WO_4 and (b) WO_3 particles. W-doping in $BiVO_4$ is based on (a) decomposition of H_2WO_4 and (b) W diffusion, respectively, during the crystallization of $BiVO_4$.

(Supporting Information Figure S3) because of the small visible light photoactivity of WO_3. Several studies[24,26] reported that a layered structure of WO_3 and $BiVO_4$ shows improved photoactivity by enhancing charge separation and transport. Films that have WO_3 in this study, however, are a simple mixed composite (Supporting Information Figure S4a), where WO_3 sites in the $BiVO_4$ film increases recombination at the WO_3/$BiVO_4$ interfaces since the band positions of two semiconductors are not properly aligned for efficient charge transport through $BiVO_4$–WO_3–$BiVO_4$ interfaces (Supporting Information Figure S4b). In contrast, WO_3 in a film of W-$BiVO_4$ shows significant improvement of performance over the undoped material. A similar effect, where the addition of graphene oxide improves the performance of $BiVO_4$, but not of W-$BiVO_4$, has been reported.[48] Besides the enhanced photoactivity, the addition of H_2WO_4 also improved the reproducibility of film preparation and film uniformity, which is shown as the precision variation in Figure 5.

There are several ways to incorporate H_2WO_4 particles into the deposited film during the electrodeposition process. H_2WO_4 is insoluble and the H_2WO_4 precursor used was bulky enough (diameter 10 μm) to settle to the bottom of the solution under nonstirred conditions. Because the FTO substrate was placed on the bottom of the electrochemical cell, the settled particles were included in the film. However, particle incorporation was also observed with the substrate electrode positioned vertically in the cell (Supporting Information Figure S5), so particle settling cannot account for all of the incorporated particles. Another driving force for particle incorporation is the attraction of particles by electrostatic forces, as seen in electrophoretic deposition. The surface charge of the particles is thus an important factor in composite deposition.[41,44] The isoelectric point (IEP) (pH) of WO_3 and H_2WO_4 is 0.5[49] and 0.43,[50] respectively, so these particles would have a negative surface charge in the plating solution (pH 5) and, accordingly, would be attracted to the substrate when it is passing an anodic current, as reported previously for the electrophoretic deposition of WO_3.[51]

Electrolyte capture is an additional way of particle incorporation. In electrodeposition, the small volume of electrolyte can be captured during the film growth and generates a few ppm level of impurities,[39] which implies that particles can be captured at the same time. This effect was investigated by using Na_2WO_4 as a soluble W source in the electrolyte as it was expected that WO_4^{2-} ions would be captured into film during electrodeposition (Supporting Information Figure S6). However, the small increase in the photoactivity and structural deformation compared to the response with H_2WO_4 indicated that the captured electrolyte amount was insignificant.

$BiVO_4$ Deposited with WO_3 Particles. Since, H_2WO_4 is the hydrated form of WO_3 and both have almost the same IEP, WO_3 can be a substitutive source of W doping in the plating electrolyte. At the same time, the deposition of a composite with WO_3 is easier to explain compared to mixed $BiVO_4$–WO_3 composite. Figure 6 shows the photoactivity and the crystal structure of $BiVO_4$ film electrodeposited with both WO_3 bulk particles (diameter $\leq$ 20 μm) and nanoparticles (NP, primary particle diameter 20 nm, which is about same as the size of WO_3 generated form H_2WO_4). One would expect nanoparticles to show better doping behavior than the larger particles with respect to uniformity of incorporation and feasibility of the penetration into the $BiVO_4$ crystal, and this is indeed consistent with the experimental results. The addition of large WO_3 particles did not create a significant increase in photocurrent, whereas WO_3 NP addition led to a sharp increase as well as the XRD peak shift that is critical evidence of W-doping in $BiVO_4$ (Figure 6a–c), resembling the addition of H_2WO_4. The difference between the films grown with WO_3 NPs and H_2WO_4 is that the $BiVO_4$ film with WO_3 NPs always shows a separate WO_3 phase, even when the critical doping concentration is not reached where the photocurrent is saturated. Figure 6d shows the shift values of characteristic XRD peak at around 47° as a function of the amount of H_2WO_4 and WO_3 NPs. It can be used as an indicator of doping level since it is approximately proportional to the doping level.[22] The addition of either type of particle increased the peak shift, indicating the development of higher doping amounts. The extent of shift for WO_3 NPs was smaller than that for H_2WO_4, which indicates that the amount of doping caused by WO_3 NPs is smaller than that by H_2WO_4. This may be due to the difference in the doping procedure at the post-heat treatment step.

In fact, as-grown electrodeposited film is amorphous and consists of Bi, V, and O, whereby annealing is essential for the formation of monoclinic $BiVO_4$ crystal that shows good PEC behavior.[29] When H_2WO_4 particles are embedded in the film and are treated at a high temperature, these particles start to decompose at 100 °C with the release of intercalated water molecules,[52] thus generating very small particles at the single molecule level. These can be readily incorporated into $BiVO_4$ and create the doping level during the crystallization (illustrated in Figure 7a). However, WO_3 NPs do not go through such a change during annealing. NPs generally have a low melting

dx.doi.org/10.1021/jp408619u | J. Phys. Chem. C 2013, 117, 23048–23056

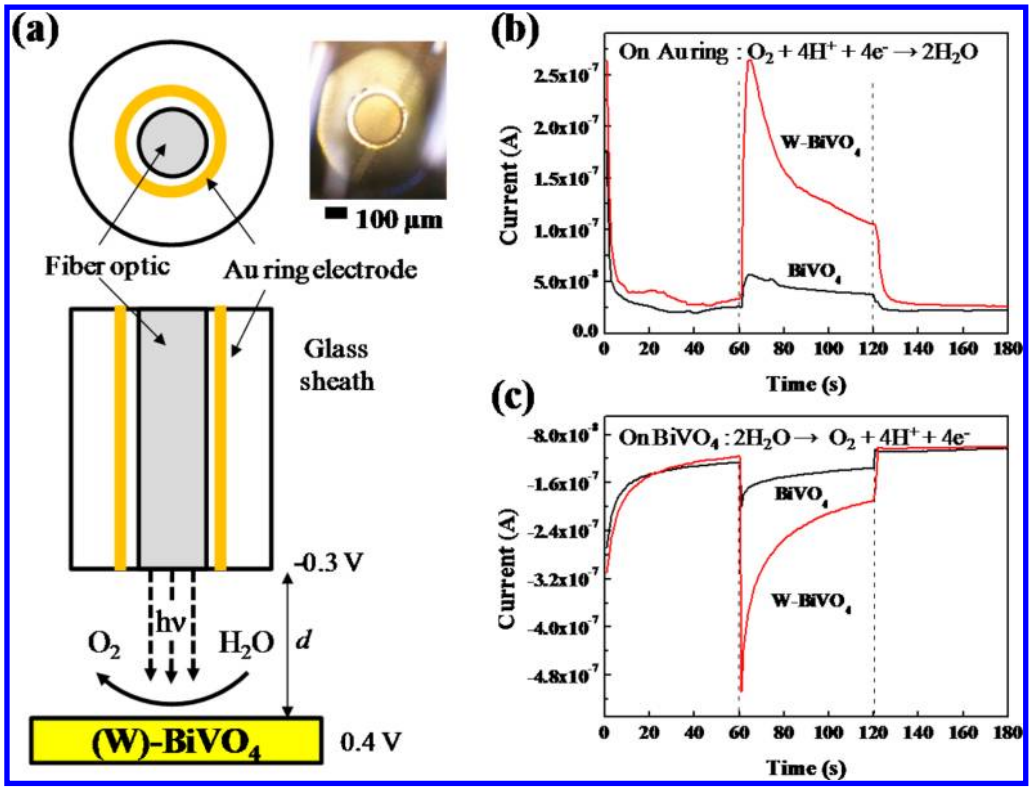

Figure 8. (a) Schematic diagram of the TC/SG mode of SECM for detection of oxygen, which is generated by the photoelectrochemical water oxidation on $BiVO_4$ under irradiation, by its reduction on Au ring electrode and chronoamperograms of (b) Au ring electrode tip collection and (c) substrate generation for water oxidation on $BiVO_4$ (black) and W-doped $BiVO_4$ (red) electrodes in 0.2 M sodium phosphate buffered aqueous solution (pH 7). The measurements started in the dark and UV–vis light began to be irradiated at 60 s and finished at 120 s.

point (mp) compared to bulk particles because of the high surface area/volume ratio,[53] and the mp of WO_3 NP (≥20 nm) used in this study was estimated to be at least 780 °C (see Supporting Information for details), which is 200 °C above the annealing temperature used. Therefore, a reasonable doping process for WO_3 particle would be the atomic diffusion of W from WO_3 to adjacent $BiVO_4$, which is usually used for the synthesis of single phase oxide from the mixture of oxides by sintering at high temperature (Figure 7b). As sintering is generally carried out at over 1000 °C and the W atom has a very small diffusion coefficient through a crystal lattice ($D_0 \approx 10^{-17}$ cm^2/s at 550 °C in α-Fe),[54] the annealing temperature is not expected to be high enough for W to diffuse sufficiently into $BiVO_4$. Unfortunately, the annealing temperature cannot exceed the softening temperature of FTO (~700 °C), and a longer annealing time (up to 9 h) did not make an observable difference in the photocurrent measured on the annealed electrodes. Because of this difficulty in the doping process using NPs, the amount of WO_3 added to optimize the photoelectrodes for the highest photocurrent was different from that of H_2WO_4 (25 mg/L for H_2WO_4 and 116 mg/L for WO_3, respectively, Figures 5 and 6b). A higher amount of precursor WO_3 addition into the deposition solution (compared to that of H_2WO_4) was needed to optimize the resulting W-doped $BiVO_4$ electrodes. However, XRD analysis indicated that the addition of WO_3 particles in the deposition solution always yields a $BiVO_4$ film with incorporated WO_3. This gives us more apparent and simple $BiVO_4$–WO_3 composite compared to $BiVO_4$–H_2WO_4, and the deteriorative effect of WO_3 embedded in $BiVO_4$ film was also observed beyond maximum doping (Figure 6b), which can be clear evidence that WO_3 generated from H_2WO_4 caused a slight decline in the photocurrent of $BiVO_4$–H_2WO_4 (Figure 5). On the basis of this explanation, better doping behavior is expected with smaller WO_3 NPs, e.g., with a size less than 10 nm, as the doping source, assuming the smaller NPs melt at a lower annealing temperature than larger particles and more easily diffuse into the $BiVO_4$.

Mo is another reported dopant in $BiVO_4$ that improves the PEC perfromance,[22] and its doping was attempted by adding molybdic acid ($MoO_3 \cdot H_2O$, IEP ≈ 2[55]) in the plating solution. A slight increase in the photocurrent was found with its addition (Supporting Information Figure S7), but its effect was not as obvious as that of H_2WO_4 or WO_3.

Detection of Evolved Oxygen by SECM. The detection of the amount of evolved oxygen is a more direct way of demonstrating better activity for PEC water oxidation since the observed photocurrent could also include oxidation of the semiconductor material itself or reduced species in the solution. Thus, the enhanced oxygen evolution by addition of H_2WO_4 was also analyzed by using SECM. The detection of oxygen produced from water oxidation at photoelectrodes under irradiation has been previously demonstrated by using the tip collection/substrate generation mode of SECM (TC/SG-SECM),[28,45] and Cong et al.[46] performed SECM in a quantitative way such as the calculation of the faradaic efficiency of oxygen evolution via numerical simulation.

The same experimental scheme presented previously[45] was used in this study for oxygen detection as illustrated in Figure 8a. First, a Au ring (plated with Pt) optical fiber disk electrode (ROFDE) approaches the substrate photoelectrode. The position of the Au-ROFDE tip was controlled by an *xyz*-stepper motor (T-LA28A, Zaber Technologies Inc., Vancouver,

dx.doi.org/10.1021/jp408619u | J. Phys. Chem. C 2013, 117, 23048–23056

Canada) on SECM stages on a photoelectrode substrate. The tip was gently touched to the substrate at initial contact, then it was retracted using the stepper motor to control the distance between the tip and the substrate. Then, with the Xe lamp as a light source, the optical fiber was illuminated leading to water oxidation on the photoelectrode with the generated oxygen collected on the Pt-plated Au ring via the oxygen reduction reaction (ORR). Pt was plated on the Au ring to promote the kinetics of the ORR, and the formation of Pt was confirmed by the emerging proton adsorption peak on cyclic voltammetry in aqueous solution (Supporting Information Figure S8). The Au ROFDE was positioned 10 μm above the $BiVO_4$ photoelectrode. Oxygen detection was performed in 0.2 M sodium phosphate buffer applying −0.3 V (vs Ag/AgCl) to the tip with the photoelectrode substrate at 0.4 V under light illumination for the oxygen evolution reaction (OER). The tip potential used was negative enough to ensure the diffusion limited collection of oxygen on the tip electrode, and no secondary reaction, e.g., the hydrogen evolution reaction, was observed at the potential used.

Figure 8b,c show chronoamperograms of Au ring tip and $BiVO_4$ substrate where light illumination began at 60 s and ended at 120 s. As expected, a sharp rise in the substrate water oxidation current with the illumination was detected, and the increment of photocurrent at W-doped $BiVO_4$ is about three times larger than that of pure $BiVO_4$, which is consistent with the results of Figure 1b. Meanwhile, the product of the water oxidation, oxygen, was successfully collected on a ring electrode and appears as an increase in the reduction current in sync with the rising oxidation photocurrent. Both the observed current of OER at the photoelectrode and ORR at the tip show an instant response to the irradiation where the diffusion of produced oxygen from the substrate to the tip only takes a few tens of ms (diffusion time, $t = d^2/2D_o$, where d is the distance between tip and photoanode, and D_0 the diffusion coefficient of oxygen, 2×10^{-5} cm^2/s[56]). Moreover, the reduction current for oxygen evolution from W-doped $BiVO_4$ was larger than that from $BiVO_4$, which confirms that the increase in the photocurrent originated from the enhancement of the water oxidation. The collection of oxygen was performed at different distances between tip and $BiVO_4$ substrate (Supporting Information Figure S9). While the generated currents are independent of d, the collected currents decreased as d increased. The results indicate that more oxygen produced at the substrate is lost to the bulk solution by diffusion when d increases.[46] The ORR response at the tip to the instant increase of OER on the substrate also became slower due to the increase in the diffusion time as d increases. The SECM measurements show that the improved activity of W-$BiVO_4$ for water oxidation compared to undoped $BiVO_4$, and the composite deposition shown here was successfully used to make a doped metal oxide photoelectrode.

CONCLUSIONS

The addition of H_2WO_4 in the plating solution for $BiVO_4$ electrodeposition led to W doping in a $BiVO_4$ photoelectrode improving its photoactivity. W incorporation and the doping-induced crystal deformation of $BiVO_4$ were confirmed by XPS and XRD analyses. Oxide composite deposition allowed insoluble and inert H_2WO_4 particles to be incorporated in the deposit film by electrophoretic deposition because of its negative surface charge. During heat treatment, it decomposed into small WO_3 molecules that could dope the $BiVO_4$. Doping using WO_3 NPs in the deposition solution was also feasible, though doping was limited because of the slower diffusion into the $BiVO_4$ crystal. Enhanced PEC water oxidation with H_2WO_4 was also observed by SECM analysis and the detection of evolved oxygen.

ASSOCIATED CONTENT

Supporting Information

LSVs, additional CVs, and experimental results. This material is available free of charge via the Internet at http://pubs.acs.org.

AUTHOR INFORMATION

Corresponding Author

*(A.J.B.) E-mail: ajbard@mail.utexas.edu.

Notes

The authors declare no competing financial interest.

ACKNOWLEDGMENTS

We acknowledge the U.S. Department of Energy (DOE) Grant DE-FG02-09ER16119 and the Robert A. Welch Foundation (F-0021) for support of this research.

REFERENCES

(1) Kudo, A.; Omori, K.; Kato, H. A Novel Aqueous Process for Preparation of Crystal Form-Controlled and Highly Crystalline $BiVO_4$ Powder from Layered Vanadates at Room Temperature and Its Photocatalytic and Photophysical Properties. *J. Am. Chem. Soc.* **1999**, *121*, 11459−11467.

(2) Abdi, F. F.; Van de Krol, R. Nature and Light Dependence of Bulk Recombination in Co-Pi-Catalyzed $BiVO_4$ Photoanode. *J. Phys. Chem. C* **2012**, *116*, 9398−9404.

(3) Saison, T.; Chemin, N.; Chaneac, C.; Durupthy, O.; Ruaux, V.; Marley, L.; Mauge, F.; Beaunier, P.; Jolivet, J.-P. Bi_2O_3, $BiVO_4$, and Bi_2WO_6: Impact of Surface Properties on Photocatalytic Activity under Visible Light. *J. Phys. Chem. C* **2011**, *115*, 5657−5666.

(4) Bard, A. J.; Fox, M. A. Artificial Photosynthesis: Solar Splitting of Water to Hydrogen and Oxygen. *Acc. Chem. Res.* **1995**, *28*, 141−145.

(5) Kudo, A.; Miseki, Y. Heterogeneous Photocatalyst Materials for Water Splitting. *Chem. Soc. Rev.* **2009**, *38*, 253−278.

(6) Osterloh, F. E. Inorganic Materials as Catalysts for Photochemical Splitting of Water. *Chem. Mater.* **2008**, *20*, 35−54.

(7) Fujishima, A.; Honda, L. Electrochemical Photolysis of Water at a Semiconductor Electrode. *Nature* **1972**, *238*, 37−38.

(8) Gai, Y.; Li, S.-S.; Xia, J.-B.; Wei, S.-H. Design of Narrow-Gap TiO_2: A Passivated Codoping Approach for Enhanced Photoelectrochemical Activity. *Phys. Rev. Lett.* **2009**, *102*, 036402.

(9) Lin, Y.; Zhou, S.; Liu, X.; Sheehan, S.; Wang, D. TiO_2/$TiSi_2$ Heterostructures for High-Efficiency Photoelectrochemical H_2O Splitting. *J. Am. Chem. Soc.* **2009**, *131*, 2772−2773.

(10) Tian, Y.; Tatsuma, T. Mechanisms and Applications of Plasmon-induced Charge Separation at TiO_2 Films Loaded with Gold Nanoparticles. *J. Am. Chem. Soc.* **2005**, *127*, 7632−7637.

(11) Bär, M.; Weinhardt, L.; Marsen, B.; Cole, B.; Gaillard, N.; Miller, E.; Heske, C. Mo Incorporation in WO_3 Thin Film Photoanodes: Tailoring the Electronic Structure for Photoelectrochemical Hydrogen Production. *Appl. Phys. Lett.* **2010**, *96*, 032107.

(12) Seabold, J.; Choi, K.-S. Effect of a Cobalt-Based Oxygen Evolution Catalyst on the Stability and the Selectivity of Photo-Oxidation Reactions of a WO_3 Photoanode. *Chem. Mater.* **2011**, *23*, 1105−1112.

(13) Mi, Q.; Zhanaidarova, A.; Brunschwig, B. S.; Gray, H. B.; Lewis, N. S. A Quantitative Assessment of the Competition between Water and Anion Oxidation at WO_3 Photoanodes in Acidic Aqueous Electrolytes. *Energy Environ. Sci.* **2012**, *5*, 5694−5700.

(14) Jang, J. S.; Lee, J.; Ye, H.; Fan, F.-R. F.; Bard, A. J. Rapid Screening of Effective Dopants for Fe_2O_3 Photocatalysts with Scanning

Electrochemical Microscopy and Investigation of Their Photoelectrochemical Properties. *J. Phys. Chem. C* **2009**, *113*, 6719−6724.
(15) Spray, R. L.; McDonald, K. J.; Choi, K.-S. Enhancing Photoresponse of Nanoparticulate α-Fe_2O_3 Electrodes by Surface Composition Tuning. *J. Phys. Chem. C* **2011**, *115*, 3497−3506.
(16) Hu, Y.-S.; Kleiman-Shwarsctein, A.; Forman, A. J.; Hazen, D.; Park, J.-N.; McFarland, E. W. Pt-Doped α-Fe_2O_3 Thin Films Active for Photoelectrochemical Water Splitting. *Chem. Mater.* **2008**, *20*, 3803−3805.
(17) Bard, A. J. Inner-Sphere Heterogeneous Electrode Reactions. Electrocatalysis and Photocatalysis: The Challenge. *J. Am. Chem. Soc.* **2010**, *132*, 7559−7567.
(18) Tokunaga, S.; Kato, H.; Kudo, A. Selective Preparation of Monoclinic and Tetragonal $BiVO_4$ with Scheelite Structure and Their Photocatalytic Properties. *Chem. Mater.* **2001**, *13*, 4624−4628.
(19) Hanna, M. C.; Nozik, A. J. Solar Conversion Efficiency of Photovoltaic and Photoelectrolysis Cells with Carrier Multiplication Absorbers. *J. Appl. Phys.* **2006**, *100*, 074510.
(20) Zhong, D. K.; Choi, S.; Gamelin, D. R. Near-Complete Suppression of Surface Recombination in Solar Photoelectrolysis by "Co-Pi" Catalyst-Modified W:$BiVO_4$. *J. Am. Chem. Soc.* **2011**, *133*, 18370−18377.
(21) Ye, H.; Lee, J.; Jang, J. S.; Bard, A. J. Rapid Screening of $BiVO_4$-Based Photocatalysts by Scanning Electrochemical Microscopy (SECM) and Studies of Their Photoelectrochemical Properties. *J. Phys. Chem. C* **2010**, *114*, 13322−13328.
(22) Park, H. S.; Kweon, K. E.; Ye, H.; Paek, E.; Hwang, G. S.; Bard, A. J. Factors in the Metal Doping of $BiVO_4$ for Improved Photoelectrocatalytic Activity as Studied by Scanning Electrochemical Microscopy and First-Principles Density-Functional Calculation. *J. Phys. Chem. C* **2011**, *115*, 17870−17879.
(23) Jo, W. J.; Jang, J.-W.; Kong, K.-J.; Kang, H. J.; Kim, J. Y.; Jun, H.; Parmar, K. P. S.; Lee, J. S. Phosphate Doping into Monoclinic $BiVO_4$ for Enhanced Photoelectrochemical Water Oxidation Activity. *Angew. Chem., Int. Ed.* **2012**, *51*, 1−6.
(24) Hong, S. J.; Lee, S.; Jang, J. S.; Lee, J. S. Heterojunction $BiVO_4$/WO_3 Electrodes for Enhanced Photoactivity of Water Oxidation. *Energy Environ. Sci.* **2011**, *4*, 1781−1787.
(25) Saito, R.; Maiseki, Y.; Sayama, K. Highly Efficient Photoelectrochemical Water Splitting Using a Thin Film Photoanode of $BiVO_4$/SnO_2/WO_3 Multi-Composite in a Carbonate Electrolyte. *Chem. Commun.* **2012**, *48*, 3833−3835.
(26) Liang, Y.; Tsubota, T.; Mooij, L. P. A.; Van de Krol, R. Highly Improved Quantum Efficiencies for Thin Film $BiVO_4$ Photoanodes. *J. Phys. Chem. C* **2011**, *115*, 17594−17598.
(27) Su, J.; Guo, L.; Bao, N.; Grimes, C. A. Nanostructured WO_3/$BiVO_4$ Heterojunction Films for Efficient Photoelectrochemical Water Splitting. *Nano Lett.* **2011**, *11*, 1928−1933.
(28) Ye, H.; Park, H. S.; Bard, A. J. Screening of Electrocatalysts for Photoelectrochemical Water Oxidation on W-Doped $BiVO_4$ Photocatalysts by Scanning Electrochemical Microscopy. *J. Phys. Chem. C* **2011**, *115*, 12464−12470.
(29) Seabold, J. A.; Choi, K.-S. Efficient and Stable Photo-Oxidation of Water by a Bismuth Vanadate Photoanode Coupled with an Iron Oxyhydroxide Oxygen Evolution Catalyst. *J. Am. Chem. Soc.* **2012**, *134*, 2186−2192.
(30) Sayama, K.; Nomura, A.; Arai, T.; Sugita, T.; Abe, R.; Yanagida, M.; Oi, T.; Iwasaki, Y.; Abe, Y.; Sugihara, H. Photoelectrochemical Decomposition of Water into H_2 and O_2 on Porous $BiVO_4$ Thin-film Electrodes under Visible Light and Significant Effect of Ag Ion Treatment. *J. Phys. Chem. B* **2006**, *110*, 11352−11360.
(31) Berglund, S. P.; Rettie, A. J.; Hoang, S.; Mullins, C. B. Incorporation of Mo and W into Nanostructured $BiVO_4$ Films for Efficient Photoelectrochemical Water Oxidation. *Phys. Chem. Chem. Phys.* **2012**, *14*, 7065−7075.
(32) Jia, Q.; Iwashina, K.; Kudo, A. Facile Fabrication of an Efficient $BiVO_4$ Thin Film Electrode for Water Splitting under Visible Light Irradiation. *Proc. Natl. Acad. Sci. U.S.A.* **2012**, *109*, 11564−11569.
(33) Su, J. Z.; Guo, L. J.; Yoriya, S.; Grimes, C. A. Aqueous Growth of Pyramidal-Shaped $BiVO_4$ Nanowire Arrays and Structural Characterization: Application to Photoelectrochemical Water Splitting. *Cryst. Growth Des.* **2010**, *10*, 856−861.
(34) Iwase, A.; Kudo, A. Photoelectrochemical Water Splitting Using Visible-Light-Responsive $BiVO_4$ Fine Particles Prepared in an Aqueous Acetic Acid Solution. *J. Mater. Chem.* **2010**, *20*, 7536−7542.
(35) Yu, J. Q.; Kudo, A. Hydrothermal Synthesis of Nanofibrous Bismuth Vanadate. *Chem. Lett.* **2005**, *34*, 850−851.
(36) Dunkle, S. S.; Helmich, R. J.; Suslick, K. S. $BiVO_4$ as a Visible-Light Photocatalyst Prepared by Ultrasonic Spray Pyrolysis. *J. Phys. Chem. C* **2009**, *113*, 11980−11983.
(37) Myung, N. M. N.; Ham, S.; Choi, S.; Chae, Y.; Kim, W. G.; Jeon, Y. J.; Paeng, K. J.; Chanmanee, W.; de Tacconi, N. R.; Rajeshwar, K. Tailoring Interfaces for Electrochemical Synthesis of Semiconductor Films: $BiVO_4$, Bi_2O_3, or Composites. *J. Phys. Chem. C* **2011**, *115*, 7793−7800.
(38) Kleiman-Shwarsctein, A.; Hu, Y.-S.; Forman, A. J.; Stucky, G. D.; McFarland, E. W. Electrodeposition of α-Fe_2O_3 Doped with Mo or Cr as Photoanodes for Photocatalytic Water Splitting. *J. Phys. Chem. C* **2008**, *112*, 15900−15907.
(39) Dini, J. W. In *Modern Electroplating*, 4th ed.; Schlesinger, M., Paunovic, M., Eds.; Wiley: New York, 2000.
(40) Maurin, G.; Lavanant, A. Electrodeposition of Nickel/Silicon Carbide Composite Coatings on a Rotating Disc Electrode. *J. Appl. Electrochem.* **1995**, *25*, 1113−1121.
(41) Hovestad, A.; Janssen, L. J. J. Electrochemical Codeposition of Inert Particles in a Metallic Matrix. *J. Appl. Electrochem.* **1995**, *25*, 519−527.
(42) Musiani, M. Anodic Deposition of PbO_2/Co_3O_4 Composites and Their Use as Electrodes for Oxygen Evolution Reaction. *Chem. Commun.* **1996**, 2403−2404.
(43) Casellato, U.; Cattarin, S.; Guerriero, P.; Musiani, M. M. Anodic Synthesis of Oxide−Matrix Composites. Composition, Morphology, and Structure of PbO_2−Matrix Composites. *Chem. Mater.* **1997**, *9*, 960−966.
(44) Jung, A.; Natter, H.; Hempelmann, R.; Lach, E. Nanocrystalline Alumina Dispersed in Nanocrystalline Nickel: Enhanced Mechanical Properties. *J. Mater. Sci.* **2009**, *44*, 2725−2735.
(45) Lee, J.; Ye, H.; Pan, S.; Bard, A. J. Screening of Photocatalysts by Scanning Electrochemical Microscopy. *Anal. Chem.* **2008**, *80*, 7445−7450.
(46) Cong, Y.; Park, H. S.; Wang, S.; Dang, H. X.; Fan, F.-R. F.; Mullins, C. B.; Bard, A. J. Synthesis of Ta_3N_5 Nanotube Arrays Modified with Electrocatalysts for Photoelectrochemical Water Oxidation. *J. Phys. Chem. C* **2012**, *116*, 14541−14550.
(47) Bard, A. J.; Mirkin, M. V. *Scanning Electrochemical Microscopy*; Marcel Dekker: New York, 2001.
(48) Park, H. S.; Ha, H.-W.; Ruoff, R. S.; Bard, A. J. On the Improvement of Photoelectrochemical Performance and Finite Element Analysis of Reduced Graphene Oxide−$BiVO_4$ Composite Electrodes. *J. Electroanal. Chem.* **2013**, DOI: 10.1016/j.jelechem.2013.08.036.
(49) Park, G. A. The Isoelectric Points of Solid Oxides, Solid Hydroxides, and Aqueous Hydroxo Complex Systems. *Chem. Rev.* **1965**, *65*, 177−198.
(50) El Wakkad, S. E. S.; Rizk, H. A. The Polytungstates and the Colloidal Nature and the Amphoteric Character of Tungstic Acid. *J. Phys. Chem.* **1957**, *61*, 494−497.
(51) Lee, S. H.; Deshpande, R.; Parilla, P. A.; Jones, K. M.; To, B.; Mahan, A. H.; Dillon, A. C. Crystalline WO_3 Nanoparticles for Highly Improved Electrochromic Applications. *Adv. Mater.* **2006**, *18*, 763−766.
(52) Nogueira, H. I. S.; Cavaleiro, A. M. V.; Rocha, J.; Trindade, T.; Pedrosa, J. D. Synthesis and Characterization of Tungsten Trioxide Powders Prepared from Tungstic Acids. *Mater. Res. Bull.* **2004**, *39*, 683−693.

(53) Jackson, C. L.; McKenna, G. B. The Melting Behavior of Organic Materials Confined in Porous Solids. *J. Chem. Phys.* **1990**, *93*, 9002−9011.
(54) Takemoto, S.; Nitta, H.; Iijima, Y.; Yamazaki, Y. Diffusion of Tungsten in α-Iron. *Philos. Mag.* **2007**, *87*, 1619−1629.
(55) Regalbuto, J. R.; Ha, J.-W. A Corrected Procedure and Consistent Interpretation for Temperature Programmed Reduction of Supported MoO_3. *Catal. Lett.* **1994**, *29*, 189−207.
(56) Ferrell, R. T.; Himmelblau, D. M. Diffusion Coefficients of Nitrogen and Oxygen in Water. *J. Chem. Eng. Data* **1967**, *12*, 111−115.